ChemSusChem

"Nailing" Redox-active Polyoxometalates (POMs) to Polypyrrole Nano-pipes for Ultrahigh Energy Density Supercapacitors

--Manuscript Draft--

Manuscript Number:	
Article Type:	Full Paper
Corresponding Author:	Deepak Dubal, Ph.D. Spain Barcelona, SPAIN
Corresponding Author E-Mail:	dubaldeepak2@gmail.com
Order of Authors (with Contributor Roles):	Deepak Dubal, Ph.D.
	Pedro Gomez-Romero
Keywords:	Polypyrrole Nanopipes, Polyoxometalates, Nanocomposite, Supercapacitors
Manuscript Classifications:	Batteries; Conducting polymers; Electrode materials; Energy storage; Supercapacitors
Suggested Reviewers:	Keryn Lian keryn.lian@utoronto.ca Expert in Polyoxometalates based Supercapacitors
	Rudolf Holze rudolf.holze@chemie.tu-chemnitz.de Expert in Polymer based supercapacitors
	Carsten Streb carsten.streb@uni-ulm.de
	Yuping Wu wuyp@fudan.edu.cn
Opposed Reviewers:	
Abstract:	Hybrid materials are prominent role-models for the fabrication of high performance supercapacitors. Here, we have explored organic-inorganic hybrid materials based on open-end porous 1D polypyrrole nano-pipes (PPy) and heteropolyoxometalate (phosphotungstate ([PW12O40]3- (PW12) or phosphomolybdate [PMo12O40]3- (PMo12)) that display excellent areal capacitances. Two different hybrid materials (PMo12@PPy and PW12@PPy) were effectively synthesized and applied for symmetric supercapacitors. The anchoring of the inorganic nanoclusters onto the conducting polymer nanopipes led indeed to electrodes which stood up to our best expectations exhibiting outstanding areal capacitances of 434 mF/cm2 for PW12@PPy and 374 mF/cm2 for PMo12@PPy respectively, which are almost 1.5 to 2 fold higher than that for pristine PPy nano-pipes (235 mF/cm2). In addition, symmetric cells based on PMo12@PPy and PW12@PPy hybrid electrodes were fabricated which showed significant improvement in cell performance with ultrahigh volumetric capacitances in the range of 6.3-6.8 F/cm3 (considering the whole volume of the device). Indeed, they provide extended potential windows in acidic electrolytes (up to 1.5 V) which led to ultrahigh energy densities of 1.5 mWh/cm3 and 2.2 mWh/cm3 for PMo12@PPy and PW12@PPy cells, respectively. Thus, these unique organic-inorganic hybrid symmetric cells displayed extraordinary electrochemical performances far exceeding those of more complex asymmetric systems.
Author Comments:	To, The Editor, ChemSusChem Dear Editor, This letter implies online submission of new investigation entitled ""Nailing" Redox-active Polyoxometalates (POMs) to Polypyrrole Nano-pipes for Ultrahigh Energy Density Supercapacitors" Deepak P. Dubal,Pedro Gomez-Romero, for publication in ChemSusChem.

	Our group made significant contribution in the development of hybrid materials based on conducting polymers and polyoxometalates in the last decade. Indeed, the anchoring of anionic POMs within the network of cationic (p-doped) CPs led to the fabrication of hybrid materials in which the inorganic clusters kept their integrity and activity while benefiting from the conducting properties and polymeric nature of the hybrid (composite) structure. Yet, the resulting materials failed to provide their full energy-storage potential because the microstructure of the polymer matrix was not optimal, making even necessary the pre-conditioning of the hybrid electrodes in order to improve their impregnation with the electrolyte. In present investigation, for the first time, we tackle simultaneously the optimization of both composition and microstructure with outstanding results. This was done by incorporating POMs into a preformed CP nanostructure, namely PPy Nanopipes which could be described as PPy nanotubes with a large inner diameter. Briefly, we have designed and fabricated unique and exceptional organic-inorganic hybrid nanocomposite materials based on highly porous 1D polypyrrole Nano-pipes (PPy) and polyoxometalates (POMs). Two different POMs (phosphotungstate (PW12) or phosphomolybdate (PMo12)) were effectively nailed on inner and outer walls of highly porous PPy Nano-pipes. Strikingly, these electrodes showed excellent areal capacitances of 434 mF/cm2 for PW12@PPy and 374 mF/cm2 for PMo12@PPy, respectively which are almost 1.5 to 2 fold higher than that for pristine PPy Nano-pipes (235 mF/cm2). Furthermore, the symmetric cells based on PMo12@PPy and PW12@PPy could be successfully cycled up to 1.3 V and 1.5 V, respectively and exhibited ultrahigh volumetric capacitance in the range of 6.3-6.8 F/cm3 (considering volume of whole device). Thus, the combination of extra capacitance and widened voltage window, together with the conductivity and optimized microstructure of the CP matrix, made of these truly synergic electrode materials, reaching remarkable energy densities of 1.5 mWh/cm3 and 2.2 mWh/cm3 for PMo12@PPy and PW12@PPy cells, respectively. I really hope you will agree that this excellent report could be a important article for many interesting reports to come. I look forward to your news
Section/Category:	
Additional Information:	
Question	**Response**
Dedication	No
Submitted solely to this journal?	Yes
Has there been a previous version?	No

“Nailing” Redox-active Polyoxometalates (POMs) to Polypyrrole Nano-pipes for Ultrahigh Energy Density Supercapacitors

Deepak P. Dubal, Pedro Gomez-Romero,***

[a]Catalan Institute of Nanoscience and Nanotechnology (ICN2), CSIC and The Barcelona Institute of Science and Technology, Campus UAB, Bellaterra, 08193 Barcelona, Spain

CORRESPONDING AUTHOR FOOTNOTE

Dr. Deepak Dubal, and Prof. Pedro Gomez-Romero

Tel.: +349373609/+34937373608 Fax: + 34936917640

E-mail: dubaldeepak2@gmail.com (D. Dubal),

pedro.gomez@cin2.es (P. Gomez-Romero)

Abstract

Hybrid materials are prominent role-models for the fabrication of high performance supercapacitors. Here, we have explored organic-inorganic hybrid materials based on open-end porous 1D polypyrrole nano-pipes (PPy) and heteropolyoxometalate (phosphotungstate ($[PW_{12}O_{40}]^{3-}$ (PW_{12}) or phosphomolybdate $[PMo_{12}O_{40}]^{3-}$ (PMo_{12})) that display excellent areal capacitances. Two different hybrid materials (PMo_{12}@PPy and PW_{12}@PPy) were effectively synthesized and applied for symmetric supercapacitors. The anchoring of the inorganic nanoclusters onto the conducting polymer nanopipes led indeed to electrodes which stood up to our best expectations exhibiting outstanding areal capacitances of 434 mF/cm^2 for PW_{12}@PPy and 374 mF/cm^2 for PMo_{12}@PPy respectively, which are almost 1.5 to 2 fold higher than that for pristine PPy nano-pipes (235 mF/cm^2). In addition, symmetric cells based on PMo_{12}@PPy and PW_{12}@PPy hybrid electrodes were fabricated which showed significant improvement in cell performance with ultrahigh volumetric capacitances in the range of 6.3-6.8 F/cm^3 (considering the whole volume of the device). Indeed, they provide extended potential windows in acidic electrolytes (up to 1.5 V) which led to ultrahigh energy densities of 1.5 mWh/cm^3 and 2.2 mWh/cm^3 for PMo_{12}@PPy and PW_{12}@PPy cells, respectively. Thus, these unique organic-inorganic hybrid symmetric cells displayed extraordinary electrochemical performances far exceeding those of more complex asymmetric systems.

Keywords: Polypyrrole Nanopipes, Polyoxometalates, Nanocomposite, Supercapacitors

Introduction

Nanostructure turned capacitors from circuitry elements into energy-storage devices. Indeed, Double Layer Capacitors (DLCs) benefit from porosity in the nanometer scale to increase their active area and decrease the charge separation distance to dimensions which make it possible for single compact devices to feature Farads instead of pico- to micro-Farads typical of conventional capacitors. Supercapacitor can nowadays provide high power with excellent cycling stability which makes them fascinating electrochemical energy storage device for many and diverse applications from small-scale portable electronics to large-scale grid-load leveling [1-3]. Yet, despite a few decades of important development, the main inadequacy of supercapacitors is still their low energy density and hence further research on new electrode materials with enhanced performance is still intensely pursued. Upgraded energy storage properties (both specific (normalized by weight) and volumetric (normalized by volume)) are essential to meet the increasingly demanding desires of the industry, and they have to be topped with low manufacturing costs and environmental friendliness [4-6]. Recent commercial supercapacitors based on activated carbons exhibit high specific capacitances of 100-150 F/g, but their low energy density limits their applications [7, 8]. It is thus needed to find new electrode materials which could provide an exceptional combination of electrochemical properties such as high capacitance and energy with sustained power and long cycle life.

Hybrid materials provide unique opportunities for the development of supercapacitor electrodes by delivering synergies and bringing together complementary properties of their components. [9, 10]. In particular, they allow for high capacitance and high energy-densities by their merging of conductivity and energy storage properties, allowing in the best cases to have capacitive and faradaic mechanisms reinforce each other [11-14]. The challenging task is to design new hybrid materials that maintains or upgrades the best properties of each material while removing or lowering their particular drawbacks. In this context, conducting polymers (CPs) are well-known multifunctional organic materials used as capacitive electrodes for

supercapacitors [15, 16] showing great versatility for the development of hybrids. Thus, CPs can be used as best materials to nail redox active molecules and prepare flexible, conducting electroactive materials through a great variety of approaches, from covalent to ionic bonding to the formation of Van der Walls adducts.

Molecular metal-oxide nanoclusters known as polyoxometalates (POMs) are an exceptional group of inorganic redox-active materials which can be considered as oxide quantum dots [17] and are recently investigated as active sites in a large number of CPs [11, 18]. Polyoxometalates (POMs) form a very large family of anionic metal-oxide clusters of different sizes and compositions. [19-21]. Nonetheless, the best known, most stable and the ones we will deal with in the present work are solid acids (or anions in their de-protonated form) with the general formula $Hn[AM_{12}O_{40}]$ (M = V, Mo, W). POMs are expected to achieve excellent electrochemical properties due to their rapid as well as extremely reversible redox reactions. Notably, POM clusters (simple Keggin type) phosphomolybdate (PMo_{12}) or phosphotungstate (PW_{12}) represent the great ability of attachments due to the presence of all 12 MO_6 moieties (Mo or W) at the surface of the cluster which makes them ultimate active materials for supercapacitors with acidic electrolytes [22-26]. Indeed, the development of hybrid materials made of CPs and POMs has been tackled by our group [11] and others [15] in the last decade. Indeed, the decoration of anionic POMs within the network of cationic (p-doped) CPs directed to the synthesis of unique hybrid materials where the redox active POM clusters maintains their electrochemical activities whereas benefiting from the conducting and polymeric properties of the hybrid material [11]. Yet, the resulting materials failed to provide their full energy-storage potential because the microstructure of the polymer matrix was not optimal, making even necessary the pre-conditioning of the hybrid electrodes in order to improve their impregnation with the electrolyte [11].

In this paper, for the first time, we tackle simultaneously the optimization of both composition and microstructure with outstanding results. This was done by incorporating POMs

into a preformed CP nanostructure, namely PPy Nanopipes which could be described as PPy nanotubes with a large inner diameter.

We have successfully designed and prepared organic-inorganic hybrid nanocomposite materials based on highly porous 1D polypyrrole Nano-pipes (PPy) and polyoxometalates (POMs). Two different POMs (phosphotungstate (PW_{12}) or phosphomolybdate (PMo_{12})) were effectively nailed on inner and outer walls of highly porous PPy Nano-pipes. These materials will be labeled as PW_{12}@PPy and PMo_{12}@PPy, respectively. Later, these hybrid materials were used as electrodes for symmetric supercapacitors. Strikingly, these electrodes showed maximum areal capacitances of 434 mF/cm^2 for PW_{12}@PPy and 374 mF/cm^2 for PMo_{12}@PPyrespectively, which are almost 1.5 to 2 fold higher than that for pristine PPy Nano-pipes (235 mF/cm^2). In addition, the symmetric cells based on PMo_{12}@PPy and PW_{12}@PPy could be successfully cycled up to 1.3 V and 1.5 V respectively, and exhibited ultrahigh volumetric capacitance in the range of 6.3-6.8 F/cm^3 (volume of device). Thus, the blending of extra capacitance and extended voltage range, together with the conductivity and optimized microstructure of the CP matrix, made of these truly synergic electrode materials, reaching remarkable energy densities of 1.5 mWh/cm^3 and 2.2 mWh/cm^3 for PMo_{12}@PPy and PW_{12}@PPy cells, respectively.

Experimental section

Synthesis of polypyrrole Nano-pipes (PPy-Npipes) and POMs@PPy hybrids

Briefly, 0.15 mmoles of Methyl Orange (MO) (i.e. sodium 4-[40 (dimethylamino)phenyldiazo]phenylsulfonate ($(CH_3)_2NC_6H_4$-N=$NC_6H_4SO_3Na$)) and 1.5 mmoles $FeCl_3$ (0.243 g) were dissolved in 30 ml de-ionized water instantly forming a flocculent precipitate. Later, 105 μL (1.5 mmoles) pyrrole was mixed to the above solution and the mixture was stirred at room temperature for next 24 h. The obtained product was then filtered and

cleaned with mixture of distilled water and ethanol and finally dried in vacuum oven at 80 °C overnight.

Later, we have prepared two hybrid materials based on PPy Nano-pipes and polyoxometalates (phosphotungstate (PW_{12}) or phosphomolybdate (PMo_{12})) symbolized as PW_{12}@PPy and PMo_{12}@PPy, hereafter. In brief, 0.15 g of above prepared PPy Nano-pipes was dispersed in deionized water (100 ml) using a bath sonicator for 30 min. In order to prepare two different hybrid materials (PW_{12}@PPy and PMo_{12}@PPy) an optimized concentration (10 mM) of phosphotungstic acid ($H_3PW_{12}O_{40}\cdot 3H_2O$, ($PW_{12}$)) or phosphomolybdic acid ($H_3PMo_{12}O_{40}\cdot 3H_2O$, ($PMo_{12}$)) was mixed with the pre-sonicated PPy-NPipes dispersion. The obtained suspension was further sonicated for 2 h and maintained for 24 h. Finally, the products were centrifuged out and dried in vacuum oven at 80 °C overnight. Fig. 1 shows schematic representation of different stages of synthesis of PW_{12}@PPy and PMo_{12}@PPy hybrid materials.

Material Characterization

The morphological analyses of hybrid materials were carried out using a field-emission scanning electron microscope (FEI Quanta 650F Environmental SEM). High resolution transmission electron microscopy (HRTEM) images and energy dispersive X-ray (EDS) spectra were acquired using an FEI Tecnai G2 F20 microscope operated at 200 kV and equipped with an EDAX super ultra-thin window (SUTW) X-ray detector. This microscope is fitted with a GIF Quantum energy filter which was used to acquire energy filtered TEM elemental maps. Maps were obtained using the three-window method on the K-edges for C and N and on the M-edges for Mo and W respectively. The composition and oxidation states of materials were investigated with X-ray photoelectron spectroscopy (XPS, SPECS Germany, PHOIBOS 150). Micromeritics instrument (Data Master V4.00Q, Serial#:2000/2400) was used to determine N_2 adsorption/desorption by Brunauer-Emmett-Teller (BET) measurements.

Electrochemical measurements

The electrodes were prepared by preparing pastes with the following composition: 85 % of active material (PPy-Npipes PW_{12}@PPy or PMo_{12}@PPy): 10 % PVDF as binder: 5 % acetylene black. In addition, N-Methyl-2-pyrrolidone (NMP, solvent) was added and the mixture was stirred for 24 h to get homogeneous paste. Finally, these pastes were coated on commercial carbon cloth by doctor-blade method and dried at 80 °C in vacuum oven for 24 h. The electrodes were cut in circular shapes of 1 cm in diameter and pressed under hydraulic press. Finally, symmetric supercapacitor cells were fabricated using Swagelok® cells with two PW_{12}@PPy and PMo_{12}@PPy electrodes of the same mass and a separator soaked with 1 M H_2SO_4 electrolyte. The cells were tested using a Biologic VMP3 potentiostat/galvanostat.

Results and Discussion

The complete growth mechanism of hollow polypyrrole Nano-pipes (PPy-Npipes) with detailed preparative parameters is explained elsewhere [27]. Briefly, $FeCl_3$ acts as a flocculant which form a fibrillary shaped solid complex with methyl orange (MO) which works as a sacrificial template. During the reaction, pyrrole is polymerized on the outer surface of the fibrillar $FeCl_3$-MO templates and forms polypyrrole Nano-pipes. This fibrillary template guided the growth of PPy and develops unique nanopipes like nanostructure while the template simultaneously degraded.

These one-dimensional hollow PPy-NPipes were used as conducting support for the adsorption of polyoxometalates (PMo_{12} or PW_{12}) (see Fig. 1). Surface morphological characterizations were carried out in order to confirm the decoration by polyoxometalates (POMs) of the surface of hollow PPy-Npipes. Fig. 2 (a, b) shows SEM images of PW_{12}@PPy and PMo_{12}@PPy nanocomposites. It is revealed that anchoring of POMs does not alter the original 1D hollow nanostructure of PPy-Npipes. Moreover, POMs@PPy-NPipes are of several micrometers in length and few nanometers in the diameter, and randomly distributed without

any aggregation. Furthermore, the size and shape of these nanopipes are investigated with zero loss peak filtered images (ZLP) and are shown in Fig. 2 (c and g). Because of the very small size (1 nm) of POM nanoparticles (PW_{12} and PMo_{12}), they are still not visible in this image. However, the PPy-NPipes exhibit outer and inner diameters of ca. 100-170 nm and 30-80 nm respectively. This implies that there is a huge (inner and outer) surface for the adsorption of POM nanoparticles. Moreover, through the open ends of these Nano-pipes, POM nanoclusters can go inside and adsorb on the inner surface of PPy-Npipes. In this way both outer and inner walls of PPy-Npipes can be utilized for the adsorption of POM nanoparticles. This hypothesis is further confirmed by EFTEM elemental mapping of PW_{12}@PPy and PMo_{12}@PPy samples. Fig. 2 (d-f) shows EFTEM mapping images for PW_{12}@PPy sample. The presence of C, N from PPy-Npipes and W from PW_{12} is clearly confirmed. In addition, careful observation of W mapping image (Fig. 2 f), explicitly proves the decoration of PW_{12} on the outer and inner walls of PPy-Npipes. Similarly, the presence of Mo in addition to C and N further endorses the formation of PMo_{12}@PPy as seen in Fig. 2 (h-k). Moreover, Fig. 2 (k) shows the uniform anchoring of PMo_{12} on to outer and inner surface of PPy-Npipes. This anchoring must take place by ionic interaction of the anionic POMs with the positively charged (p-doped) PPy Nanopipes. Thus, all these surface morphological studies provide sufficient evidence for 1D nanostructuration with 1 nm-sized POMs nanoparticles densely decorating the surface (see supporting information S1). These POM-loaded 1D PPy-Nano-pipes could lead to many interesting derivations, from catalytic to sensing applications. But the unique combination of electronic properties, high electrochemically active cites, easy ionic transportation and extra-redox active material make of these materials an optimal choice for supercapacitors application.

It is very important to note that all the twelve Mo or W atoms are present on the surface of POMs (PW_{12} or PMo_{12}) molecular clusters of only 1nm size which are uniformly anchored onto the surface of PPy-NPipes. As the charge stored in pseudo-capacitive mechanism is rely on surface redox reactions i.e. the charge transfer at/or near the electrode surface, this unique

hybrid is an ultimate material for electrode/electrolyte surface polarization. Certainly, this exceptional POMs@PPy-Npipes hybrid combines a conducting 1D hollow nano-architecture with anchored PW_{12} or PMo_{12} redox active molecular clusters which provides an excellent structural foundation for high energy storage device.

Fig. 3 (a) shows full XPS spectra of PPy-Npipes, PMo_{12}@PPy and PW_{12}@PPy samples. The presence of carbon (C1s, 284.5 eV) and nitrogen (N1s, 399.6 eV) in all the three samples suggests the formation of PPy-Npipes [28]. In addition to C1s and N1s, two additional peaks at 230.5 eV and 417.5 eV are observed which corresponds to Mo3d and Mo3p, respectively from PMo_{12}@PPy whereas peaks at 39.4 eV, doublet (248.7 eV, 263.4 eV), 429.3 eV, 494.3 eV and 602.2 eV resembles to W4f, W4d, W4p and W4s, respectively from PW_{12}@PPy sample confirming the formation of hybrid materials [29, 30]. As seen from magnified view of N1s spectra (Fig. 3 b), the peak intensity is significantly decrease with a slight increase in broadness suggesting the anchoring of POMs (PMo_{12} or PW_{12}) on the surface of PPy-Npipes. The N1s peak observed at 399.6 eV corresponds to the neutral nitrogen in PPy ring (-NH-) and assigned to 'pyrrolic' nitrogen [31]. Fig. 3 (c) shows the close view of Mo3d core spectrum. The spectrum exhibits two peaks at 232.3 eV ($Mo3d_{3/2}$) and 235.4 eV ($Mo3d_{5/2}$), confirming the presence of PMo_{12} in PMo_{12}@PPy hybrid which is in the Mo(VI) oxidation state [32]. The core-level W4f spectrum shows two peaks at 37.54 eV ($W4f_{5/2}$) and 35.4 eV ($W4f_{7/2}$) with spin-orbit splitting of 2.14 eV as shown in Fig. 3 (d). It is further confirmed that the W atoms exhibits an oxidation state of W(VI) of PW_{12} in PW_{12}@PPy [33, 34].

High surface and one dimensional hollow nanostructures are ideally suited for energy storage devices. Thus, in order to check porosity and surface are of these unique hybrid nanostructures, BET analyses were carried out and the results are presented in Fig. 4. BET surface areas for PPy-Npipes, PMo_{12}@PPy and PW_{12}@PPy samples were found to be 43.11 m^2/g, 36.47 m^2/g and 34.14 m^2/g, respectively. This decrease in the BET surface areas for PMo_{12}@PPy and PW_{12}@PPy is attributed to the inclusion of the PMo_{12} and PW_{12} nanoparticles

because of their heavy contribution in the hybrid nanocomposites. Yet, the specific surface area of PMo_{12}@PPy and PW_{12}@PPy is comparable to the values reported for conducting polymers [35-37]. It is further seen that all these hybrids nanostructured PMo_{12}@PPy and PW_{12}@PPy samples exhibit meso/macroporous nature, showing a pore size range between 2-8 nm and 10-20 nm, respectively. Moreover, the pore volume of PPy-Npipes increases from 0.000685 cm^3/g to 0.0025 and 0.0031 cm^3/g after anchoring the PW_{12} and PMo_{12} inorganic clusters, respectively. This increased pore volume is highly beneficial for electrolytic ion transportation during charge/discharge mechanism. Preserving such a unique nano-architecture even after heavy loading of redox active POMs nanoparticles can efficiently provide an easy access to electrolyte ions which may significantly improve the charge transport and power capability. In addition, excellent mesoporous nature of the hybrid materials can reduce diffusion distances [38].

The electrochemical performances of PMo_{12}@PPy and PW_{12}@PPy hybrid electrodes were investigated in 1 M H_2SO_4 electrolyte using a 3-electrode cell. Cyclic voltammetry curves for PMo_{12}@PPy and PW_{12}@PPy at various scanning rates are shown in S.I. S2. The CV curves for both hybrid electrodes are quasi-rectangular with various broad redox peaks from PMo_{12} and PW_{12} overlapped with a nearly rectangular (pseudo-capacitive) envelope. This CV structure ratifies the coexistence of faradaic and pseudo-capacitive charge-storing mechanisms. Interestingly, the CV curves still maintain the redox peaks even at a high scan rate of 100 mV/s, suggesting excellent rate capability of PMo_{12}@PPy and PW_{12}@PPy for rapid charge/discharge reactions. Galvanostatic charge/discharge (GCD) curves for both PMo_{12}@PPy and PW_{12}@PPy hybrid materials are not ideal triangular shapes, further confirming the presence of dual charge-storing mechanisms (see S. I. S2). The initial voltage drops in both hybrid materials is almost negligible and also the charging part is symmetrical to the discharging part, suggesting an excellent electrochemical reversibility. Moreover, the small internal resistance (iR) loss for both hybrid electrodes may be ascribed to the mesoporous nanopipes-like nature.

The main reason for such excellent supercapacitive performances of these hybrid materials is a smart design and proper hybridizations that is a combination of optimized microstructure and composition. The advantages of these unique hybrid nanostructures are: 1) even after heavy decoration of POMs, the materials retain their original open 1D hollow nanostructure, which provides easy access to electrolyte ions 2) in addition, thin walls of PPy Nano-pipes and ultra-long lengths (several micrometers) offer low diffusion paths and large electrochemically active surface area, 3) all the twelve MoO_6 or WO_6 inorganic moieties such are at the surface and hence can make easy contact with electrolyte and take part in charge storing mechanisms.

Fig. 5 displays the effect of PW_{12} and PMo_{12} attachment to PPy-Npipes on the electrochemical performances. Figure 5 (a) shows the CV curves of PPy-Npipes, PMo_{12}@PPy and PW_{12}@PPy at constant scan rate of 10 mV/s. It is quite impressive to note the huge increase in current density for PMo_{12}@PPy and PW_{12}@PPy hybrid electrodes with additional potentials of -0.3 V (vs Ag/AgCl) and -0.5 V (vs Ag/AgCl) compared to PPy-NPipes electrodes, all of which imply a significantly larger capacitance. Fig. 5 (b) shows the maximum values of specific and areal capacitances obtained for PPy-Npipes, PMo_{12}@PPy and PW_{12}@PPy electrodes. Both hybrid electrodes exhibit high capacitances such as 434 mF/cm^2 (341 F/g) for PW_{12}@PPy and 374 mF/cm^2 (294.1 F/g) for PMo_{12}@PPy as compared to pristine PPy-Npipes (234 mF/cm^2, 204.5 F/g). Thus, a considerable increase in the capacitances of hybrid electrodes is observed which definitely can be credited to the inclusion of these redox-active inorganic POMs nanodots. Fig. 5 (c) shows the plot of variation of specific capacitance with current density for all the three samples. Remarkably, up to 63 % (for PW_{12}@PPy) and 46 % (for PMo_{12}@PPy) of the capacitance is retained, even after 10 times increase in current density (2 to 20 mA/cm^2), indicating a very good high-rate performance. Thus the slight decrease in specific capacitance of hybrid materials with current density is due to the diffusion limitations.

In order to show the potential for practical application of these hybrid electrodes, symmetric supercapacitor cells were fabricated by sandwiching H_2SO_4-soaked separators between two identical electrodes (either PMo_{12}@PPy or PW_{12}@PPy hybrid electrodes). The shapes of CV curves for both symmetric cells are not ideally rectangular as seen from Fig. 6 (a, b), suggesting inclusion of faradaic behavior of POM nanoparticles as well as pseudo-capacitive behavior of PPy-Npipes. Impressively, these symmetric cells can be easily cycled between 1.3 V for PMo_{12}@PPy and 1.5 V for PW_{12}@PPy, respectively which leads to an increased energy density. Thus, it is clear that decorated POMs nanoparticles not only add an extra capacitance but also extend the working voltage window of the device. To investigate the voltage distribution across the positive and negative electrodes, the CD curves were recorded simultaneously for two and three electrode configurations by synchronizing two channels of our potentiostat. The first channel monitors the cell in a 2-electrode mode while the second channel is connected in a 3-electrode configuration with Ag/AgCl as third (reference) electrode in order to monitor the working electrode. Fig. 6 (c, d) shows CD curves for symmetric cells based on PW_{12}@PPy and PMo_{12}@PPy, respectively at 3.3 A/g and with respect to Ag/AgCl reference electrode (red and green curves). It is revealed that the positive and negative electrodes work in the following different voltage range: +0.497 V to +1.04 V and from +0.497 to -0.451 V (vs Ag/AgCl) for PW_{12}@PPy while that for PMo_{12}@PPy cell works in the regime: +0.401 V to +0.891 V and +0.401 to -0.410 V (vs Ag/AgCl). These different working voltage regimes for positive and negative electrodes suggests different intrinsic capacitance and redox chemistries of the electrodes. Furthermore, the volumetric capacitances for our hybrid electrodes were calculated from CD curves recorded at different current densities (see S.I. S3) and are plotted in Fig. 7 (a). The PW_{12}@PPy symmetric cell offers an ultrahigh volumetric capacitance of 7.46 F/cm^3 (107.1 F/g for total mass of both electrodes (4.8 mg), here we have considered volume of whole device, 0.0689 cm^3), whereas PMo_{12}@PPy yields 6.53 F/cm^3 (97.8 F/g total mass of both electrodes (4.6 mg) at a current density of 5 mA/cm^2, respectively. It is worth noting that the

hybrid electrodes retain capacitance values of 5.2 F/cm^3 (74.6 F/g) for PW_{12}@PPy and 4 F/cm^3 (60 F/g) for PMo_{12}@PPy symmetric cell after increasing the current density from 5 mA/cm^2 to 13 mA/cm^2 , suggesting excellent rate capability (S. I. S4). This excellent enhancement in the specific capacitance is endorsed to the additional faradaic reactions of PW_{12} and PMo_{12} in the nanohybrid. The values reported here are significantly higher than those for other electrodes and cell configurations [39-43]. A summary of supercapacitive values for POMs and other electrodes are presented in S.I. S5. Fig. 7 (b, c) presents the volumetric and gravimetric Ragone plots for PW_{12}@PPy and PMo_{12}@PPy symmetric cells. Ragone plots show that the PW_{12}@PPy and PMo_{12}@PPy cells deliver maximum volumetric energy density of 2.33 mWh/cm^3 (33.5 Wh/kg) and 1.5 mWh/cm^3 (22.9 Wh/kg) at power density of 54 mW/cm^3 (781 W/kg) and 47 mW/cm^3 (706 W/kg), respectively. Moreover, at a high power density of 163 mW/cm^3 (2.3 kW/kg) and 122 mW/cm^3 (1.8 kW/kg), PW_{12}@PPy and PMo_{12}@PPy symmetric cells still provide a higher energy density of 1.6 mWh/cm^3 (23.3 Wh/kg) and 0.9 mWh/cm^3 (14.1 Wh/kg), respectively. These results demonstrate that both PW_{12}@PPy and PMo_{12}@PPy hybrid based symmetric cells are excellent energy storage systems which can provides high energy with high rates (power). The volumetric energy density reported is the highest value for PPy-based supercapacitors until now [41, 44-49]. The excellent performance can be attributed to the homogeneously nailed POMs nanodots onto the 1D hollow PPy-Nano-pipes as well as to the unique cell design coupling two charge storing mechanisms in a single electrode and in a single device.

The capacitance retention of PW_{12}@PPy and PMo_{12}@PPy symmetric cells were investigated with charge/discharge cycles at 11 mA/cm^2 current density and presented in Fig. 7 (d). Strikingly, both PW_{12}@PPy and PMo_{12}@PPy cells show good capacity retention of 83-84 % over 5000 cycles. Despite the common problem of capacitance degradation in pseudo-capacitive and faradaic electrodes, PW_{12}@PPy and PMo_{12}@PPy hybrid cells exhibit good capacity retention. The main reason for this excellent cycle life might be a synergetic effect of

pseudo-capacitive and faradaic materials. In addition, 1D hollow nanostructure of these hybrid materials is kept regardless of the volume expansion during charge/discharge cycling.

Thus, present investigation exposed that, the proper hybridization and unique nano-architecture are the keys to extract the excellent electrochemical performance from hybrid electrodes.

Conclusions

In summary, we have designed a unique, tailor-made hybrid nanostructure by nailing 1nm sized inorganic clusters (PMo_{12} and PW_{12}) ionically anchored on the walls (inner and outer) of 1D hollow nano-pipes. Furthermore, these hybrid materials showed excellent areal capacitances of 434 mF/cm^2 for PW_{12}@PPy and 374 mF/cm^2 for PMo_{12}@PPy, respectively which are almost 1.5 to 2 fold higher than that for pristine PPy nano-pipes (235 mF/cm^2). In addition, symmetric cells based on PMo_{12}@PPy and PW_{12}@PPy hybrid electrodes were assembled in order to show the practical application of these hybrid electrodes. Interestingly, the symmetric cells based on PW_{12}@PPy and PMo_{12}@PPy exhibit excellent electrochemical performance with ultrahigh volumetric capacitances in the range of 6.3-6.8 F/cm^3 (considering volume of the device) and ultrahigh energy densities of 1.5 mWh/cm^3 and 2.2 mWh/cm^3 for PMo_{12}@PPy and PW_{12}@PPy cells, respectively. Thus, these unique organic-inorganic hybrid symmetric devices displayed better electrochemical performances than complex asymmetric systems for the equal power and represent a remarkable advance towards high energy density supercapacitors.

Acknowledgments

Partial funding from Miisterio de Economía y Competitividad through Fondo Europeo de Desarrollo Regional (FEDER) (Grant MAT2015-68394-R, MINECO/FEDER) and from AGAUR (project NESTOR) are acknowledged. ICN2 acknowledges support of the Spanish MINECO

through the Severo Ochoa Centers of Excellence Program under Grant SEV-2013-0295. Finally, the award to DPD of a Marie-Curie Fellowship through Beatriu de Pinos Program (BP-DGR-2013) from the Catalan system of science and technology, Spain, is gratefully acknowledged

References

[1] D. P. Dubal, O. Ayyad, V. Ruiz, P. Gómez-Romero, *Chem. Soc. Rev.* **2015**, *44*, 1777–1790

[2] Y. Gogotsi, P. Simon, *Science* **2011**, *334*, 917-918

[3] D. P. Dubal, J. G. Kim, Y. Kim, R. Holze, C. D. Lokhande, W. B. Kim, *Energy Technol.* **2014**, *2*, 325-341

[4] P. Simon, Y. Gogotsi, B. Dunn, *Science*, **2014**, 343,1210-1211

[5] Y. Yue, H. Liang, *J. Power Sources*, **2015**, 284, 435-445

[6] Q. Zhang, E. Uchaker, S. L. Candelaria, G. Cao, *Chem. Soc. Rev.,* **2013**, 42, 3127-3171

[7] L. Dai, D. W. Chang, J. B. Baek, W. Lu, *small* **2012**, 8, 1130-1166

[8] H. Jiang, P. S. Lee, C. Li, *Energy Environ. Sci.*, **2013**, 6, 41-53

[9] P. Gomez-Romero, *Adv. Mater.* **2001**, 13, 163-174

[10] Y. Ji, L. Huang, J. Hu, C. Streb, Y. F. Song, *Energy Environ. Sci.*, **2015**, 8, 776-789

[11] P. Gomez-Romero, M. Chojak, K. Cuentas-Gallegos, J. A. Asensio, P. J. Kulesza, N. Casan-Pastor, M. Lira-Cantu, *Electrochem. Commun.* **2003**, 5, 149-153.

[12] A. K. Cuentas-Gallegos, M. Lira-Cantu, N. Casan-Pastor, P. Gomez-Romero, *Adv. Funct. Mater.* **2005**, 15, 1125-1133

[13] J. Vaillant, M. Lira-Cantu, K. Cuentas-Gallegos, N. Casan-Pastor, P. Gomez-Romero, *Prog. Sol. State Chem.* **2006**, 34, 147-159.

[14] M. Genovese, K. Lian, *Curr. Opin. Solid State Mater. Sci.* **2015**, 19, 126-137

[15] D. P. Dubal, S. H. Lee, J. G. Kim, W. B. Kim, C. D. Lokhande, *J. Mater. Chem.*, **2012**, 22, 3044-3052

[16] S. S. Shinde, G. S. Gund, D. P. Dubal, S. B. Jambure, C. D. Lokhande, Electrochim. Acta., 2014, 119, 1-10

[17] P. Gomez-Romero, *Sol. State Ionics* **1997**, 101, 243-248

[18] S. Herrmann, C. Ritchie, C. Streb, *Dalton Trans.*, **2015**, 44, 7092–7104

[19] N. Casan-Pastor, P. Gomez-Romero, *Front. Biosci.* **2004**, 9, 1759-1770.

[20] D. L. Long, R. Tsunashima, L. Cronin, *Angew. Chem. Int. Ed.* **2010**, 49, 1736-1758

[21] M. Ammam, *J. Mater. Chem. A*, **2013**, 1, 6291-6312

[22] V. Ruiz, J. Suarez-Guevara, P. Gomez-Romero, Electrochem. Commun., **2012**, 24, 35-38.

[23] J. Suarez-Guevara, V. Ruiz, P. Gomez-Romero, *J. Mater. Chem. A*, **2014**, 2, 1014-1021

[24] M. Genovese, K. Lian, *Electrochem. Commun.*, **2014**, 43, 60-62.

[25] S. Park, K. Lian, Y. Gogotsi, *J. Electrochem. Soc.*, **2009**, 156, A921-A926

[26] T. Akter, K. W. Hu, K. Lian, *Electrochim. Acta*, **2011**, 56, 4966-4971

[27] X. Yang, Z. Zhu, T. Dai, Y. Lu, *Macromol. Rapid Commun.* **2005**, 26, 1736-1740

[28] D. P. Dubal, N. R. Chodankar, Z. Caban-Huertas, F. Wolfart, M. Vidotti, R. Holze, C. D. Lokhande, P. Gomez-Romero, *J. Power Sources*, **2016**, 308 158-165

[29] J. Miao, F. X. Xiao, H. B. Yang, S. Y. Khoo, J. Chen, Z. Fan, Y. Y. Hsu, H. M. Chen, H. Zhang, B. Liu, *Sci. Adv.* **2015**, 1, e1500259

[30] Y. M. Zhao, W. B. Hu, Y. D. Xia, E. F. Smith, Y. Q. Zhu, W. Dunnill, D. H. Gregory, *J. Mater. Chem.*, 2007, 17, 4436–4440

[31] N. Su, H.B. Li, S.J. Yuan, S.P. Yi, E.Q. Yin, eXPRESS Polym. Lett. 6 (2012) 697-705

[32] A. Ma, X. Zhang, Z. Li, X. Wang, L. Ye, S. Lin, *J. Electrochem. Soc.*, **2014**, 161**,** F1224-F1230.

[33] D. Barreca, G. Carta, A. Gasparotto, G. Rossetto, E. Tondello, P. Zanella, Surf. Sci. Spectra, 2001, 8, 258

[34] L. Weinhardt, M. Blum, M. Bär, C. Heske, B. Cole, B. Marsen, E. L. Miller, J. Phys. Chem. C, 2008, 112, 3078-3082.

[35] N. Parveen, M. O. Ansari, M. H. Cho, *Ind. Eng. Chem. Res.*, **2016**, 55, 116-124

[36] R. Panigrahi, S. K. Srivastava, *Sci. Rep.* **2015***,* 5, 7638

[37] Y. Li, K. G. Neoh, L. Cen, E. T. Kang, *Langmuir* **2005**, 21, 10702-10709

[38] J. Zhang, L.B. Kong, J.J. Cai, H. Li, Y.C. Luo, L. Kang, *Microporous Mesoporous Mater.* **2010**, 132, 154-162

[39] H. Y. Chen, R. Al-Oweini, J. Friedl, C. Y. Lee, L. Li, U. Kortz, U. Stimming, M. Srinivasan*, Nanoscale*, **2015,** 7, 7934-7941.

[40] M. Skunik, M. Chojak, I. A. Rutkowska, P. J. Kulesza, *Electrochim. Acta*, **2008**, 53, 3862-3869.

[41] G. M. Suppes, C. G. Cameron, M. S. Freund, *J. Electrochem. Soc.*, **2010**, 157, A1030-A1034

[42] P. Gomez-Romero, M. Chojak, A. Cuentas-Gallegos, J. A. Asensio, P. J. Kulesza, N. Casan-Pastor, M. Lira-Cantu, *Electrochem. Commun.*, **2003**, 5, 149-153

[43] A. Cuentas-Gallegos, P. Gomez-Romero, *J. Power Sources* **2006,** *161,* 580-586

[44] Y. Su, I. Zhitomirsky, *Appl. Energy*, **2015**, 153, 48-55

[45] F. Wang, X. Zhan, Z. Cheng, Z. Wang, Q. Wang, K. Xu, M. Safdar, J. He, *small*, **2015**, 11, 749-755

[46] L. Q. Fan, G. J. Liu, J. H. Wu, L. Liu, J. M. Lin, Y. L. Wei, *Electrochim. Acta*, **2014**, 137, 26-33

[47] C. Zhou, Y. Zhang, Y. Li, J. Liu, *Nano Lett.* **2013**, 13, 2078−2085

[48] Q. Qu, Y. Zhu, X. Gao, Y. Wu, *Adv. Energy Mater.* **2012**, 2, 950-955

[49] Y. J. Peng, T. H. Wu, C. T. Hsu, S. M. Li, M. G. Chen, C. C. Hu, *J. Power Sources*, **2014**, 272, 970-978

[50] D. P. Dubal, J. Suarez-Guevara, D. Tonti, E. Enciso, P. Gomez-Romero, *J. Mater. Chem. A*, **2015**, 3, 23483–23492

Figure captions

Fig. 1 Schematic illustration of steps involved in the synthesis of polypyrrole nanopipes (PPy-Npipes) and Polyoxometalates (POMs, PMo_{12} or PW_{12}) hybrid material with simple chemical method, the POM graphic is reproduced with the permission of Royal Society of Chemistry from our previous publication [50].

Fig. 2 (a, b) SEM images of PMo_{12}@PPy and PW_{12}@PPy hybrid materials, respectively, (c-f and g-k) Zero loss peak filtered image (ZLP) with corresponding EFTEM mapping for PW_{12}@PPy and PMo_{12}@PPy hybrids, respectively.

Fig. 3 (a) Full XPS spectra of PPy, PMo_{12}@PPy and PW_{12}@PPy hybrid materials (b) core-level XPS spectra of N1s of PPy, PMo_{12}@PPy and PW_{12}@PPy (c, d) core-level XPS spectra of Mo3d and W4f, respectively.

Fig. 4 (a, b) Nitrogen adsorption-desorption curves with corresponding pore size distribution plots PPy, PMo_{12}@PPy and PW_{12}@PPy samples, respectively

Fig. 5 (a) Comparative CV curves for PPy, PMo_{12}@PPy and PW_{12}@PPy samples, respectively at 10 mV/s scan rates, (b) Specific and areal capacitances of PPy, PMo_{12}@PPy and PW_{12}@PPy samples at 2 mA/cm^2, respectively (c) Variation of specific capacitance of PPy, PMo_{12}@PPy and PW_{12}@PPy samples as a function of current density.

Fig. 6 (a, b) cyclic voltammetry (CV) curves of PW_{12}@PPy and PMo_{12}@PPy based symmetric cells at different scanning rates, respectively, (c, d) Galvanostatic charge/discharge (CD) curves for PW_{12}@PPy and PMo_{12}@PPy based symmetric cells with and the corresponding positive and negative electrode profiles with respect to Ag/AgCl reference electrode.

Fig. 7 (a) Variation of volumetric capacitances for PW_{12}@PPy and PMo_{12}@PPy based symmetric cells with current densities, (b, c) Ragone plots for PW_{12}@PPy and PMo_{12}@PPy based cells, (d) Variation of specific capacitances for PW_{12}@PPy and PMo_{12}@PPy symmetric cell measured with cycling charge-discharge test at a current density of 11 mA/cm^2.

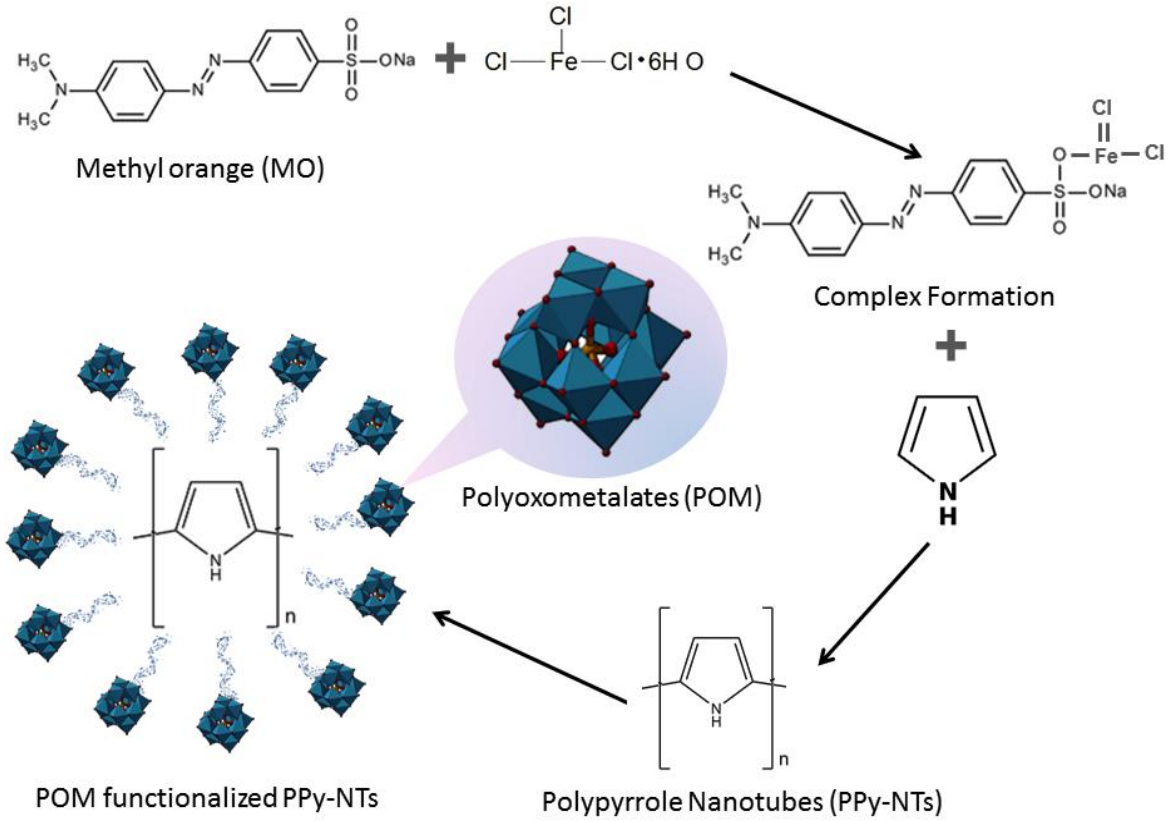
Methyl orange (MO)
Cl
Cl — Fe — Cl • 6H O
Complex Formation
Polyoxometalates (POM)
POM functionalized PPy-NTs
Polypyrrole Nanotubes (PPy-NTs)

Fig. 1

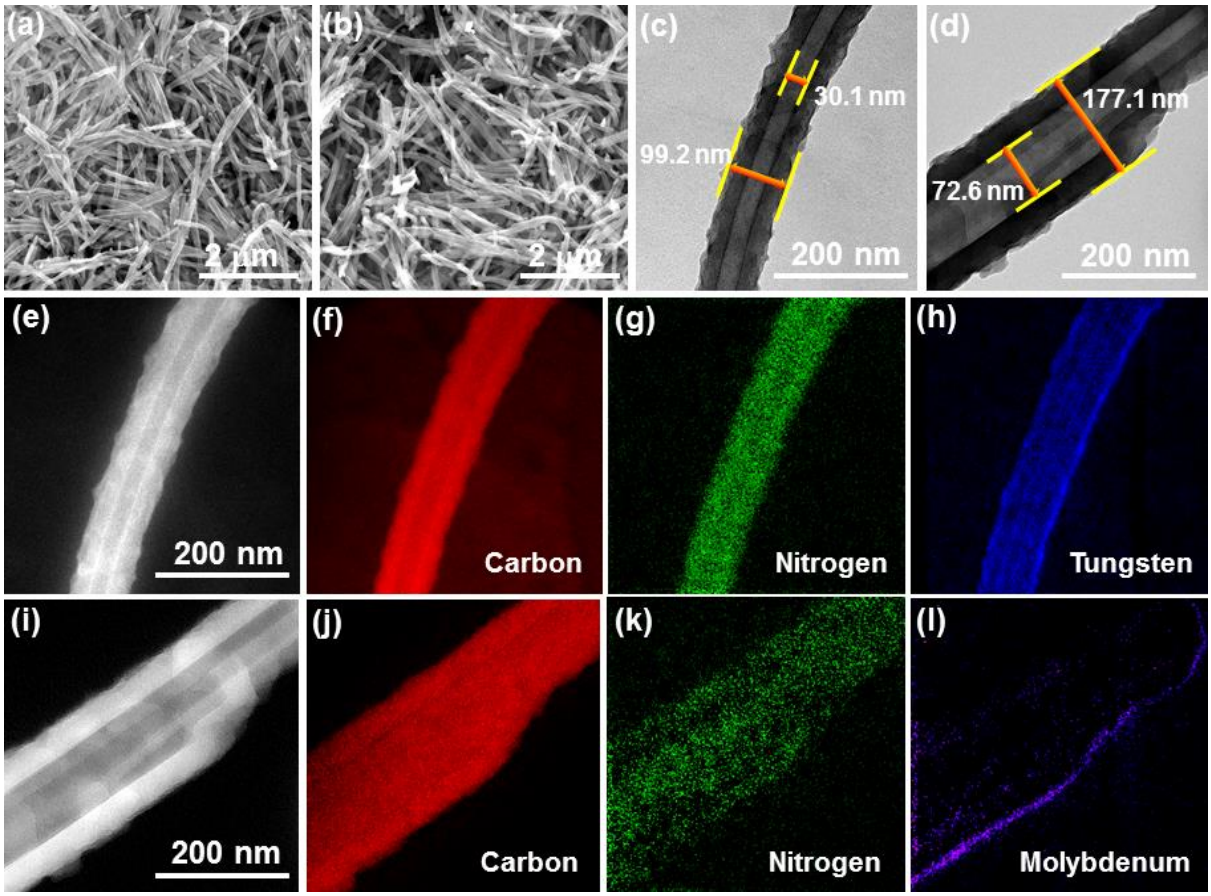
(a)
2 μm
(b)
2 μm
(c)
30.1 nm
99.2 nm
200 nm
(d)
177.1 nm
72.6 nm
200 nm
(e)
200 nm
(f)
Carbon
(g)
Nitrogen
(h)
Tungsten
(i)
200 nm
(j)
Carbon
(k)
Nitrogen
(l)
Molybdenum

Fig. 2

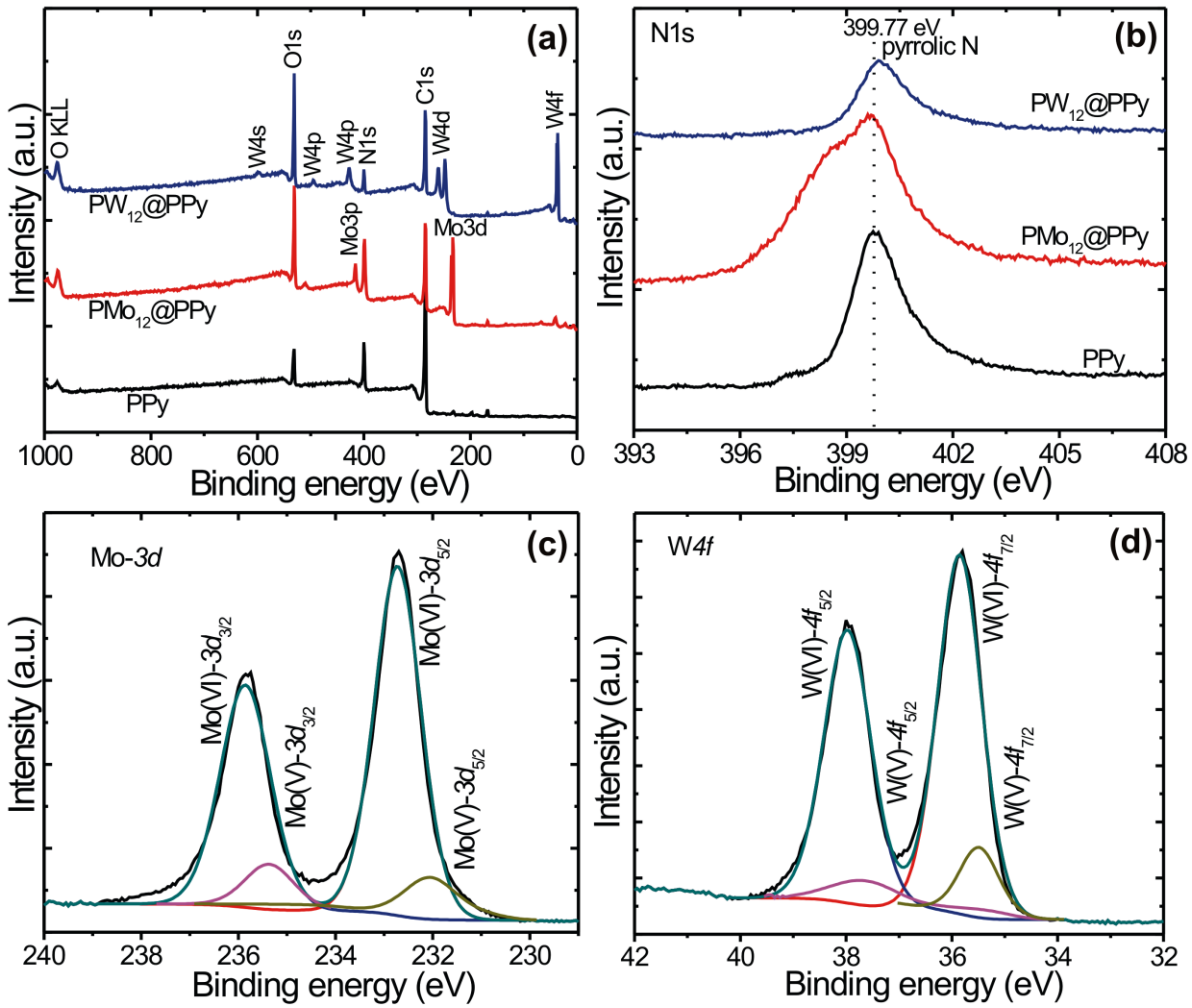
(a)
O KLL
O1s
W4s
W4p
W4p
N1s
C1s
W4d
W4f
PW12@PPy
Mo3p
Mo3d
PMo12@PPy
PPy
Intensity (a.u.)
1000
800
600
400
200
0
Binding energy (eV)
(b)
N1s
399.77 eV
pyrrolic N
PW12@PPy
PMo12@PPy
PPy
Intensity (a.u.)
393
396
399
402
405
408
Binding energy (eV)
(c)
Mo-3d
Mo(VI)-3d3/2
Mo(V)-3d3/2
Mo(VI)-3d5/2
Mo(V)-3d5/2
Intensity (a.u.)
240
238
236
234
232
230
Binding energy (eV)
(d)
W4f
W(VI)-4f5/2
W(V)-4f5/2
W(VI)-4f7/2
W(V)-4f7/2
Intensity (a.u.)
42
40
38
36
34
32
Binding energy (eV)

Fig. 3

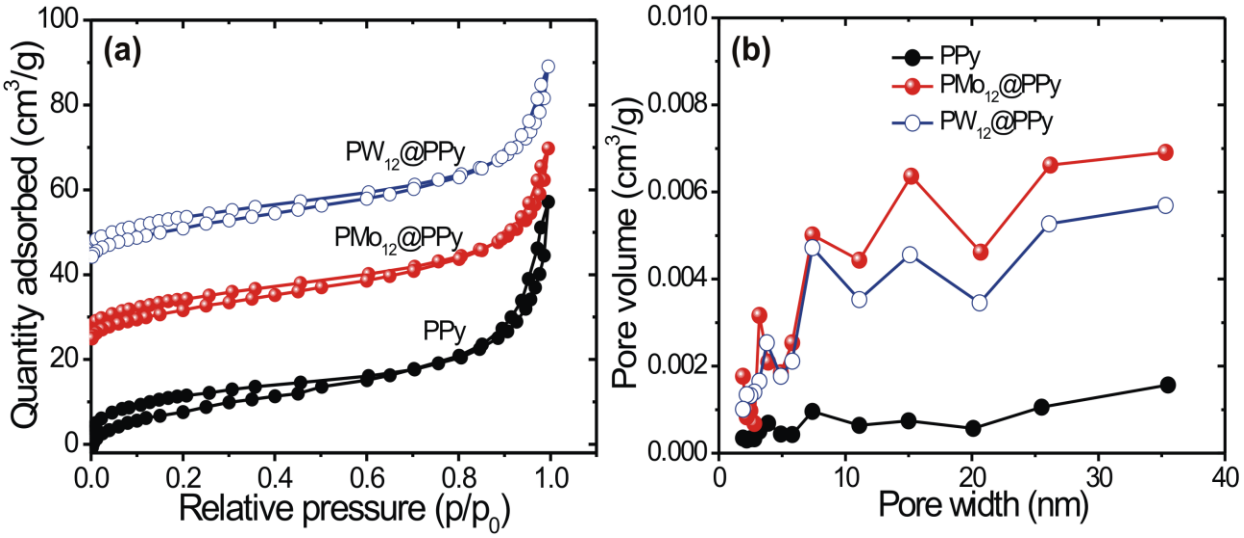
(a)
Quantity adsorbed (cm3/g)
Relative pressure (p/p0)
PW12@PPy
PMo12@PPy
PPy
(b)
Pore volume (cm3/g)
Pore width (nm)
PPy
PMo12@PPy
PW12@PPy

Fig. 4

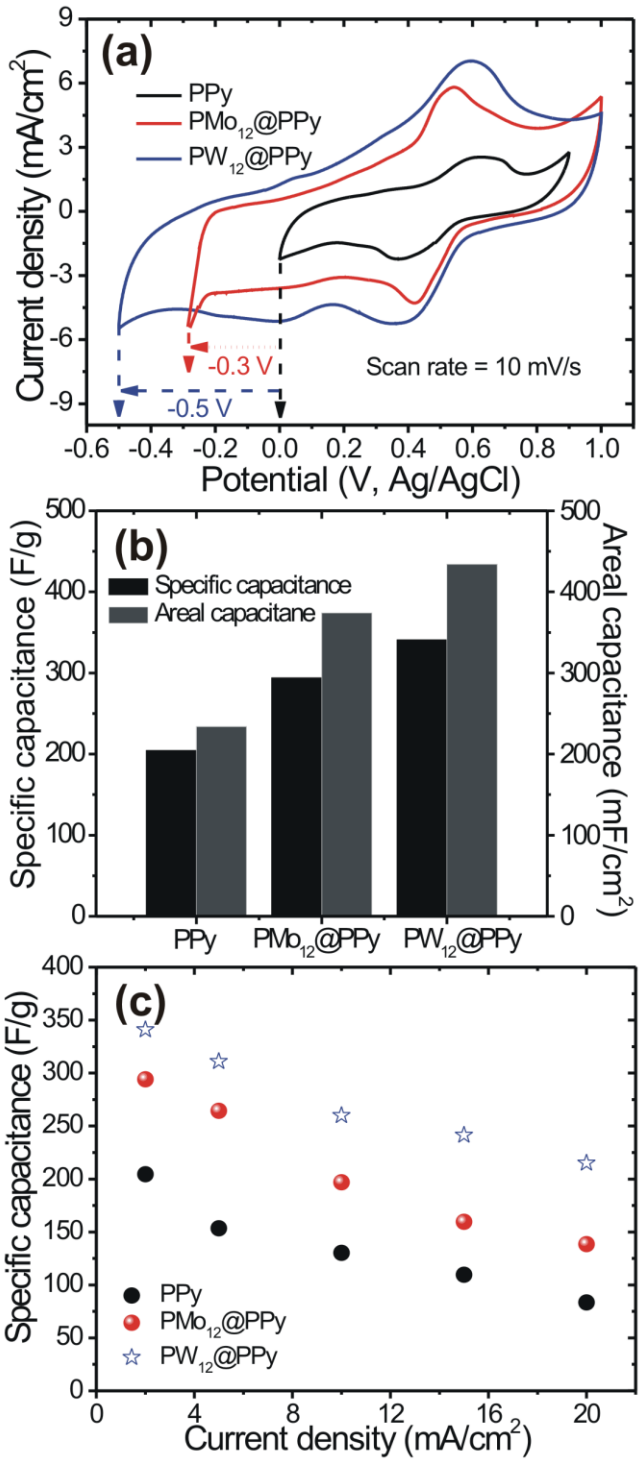
(a)
PPy
PMo12@PPy
PW12@PPy
-0.3 V
-0.5 V
Scan rate = 10 mV/s
Current density (mA/cm2)
Potential (V, Ag/AgCl)
(b)
Specific capacitance
Areal capacitane
Specific capacitance (F/g)
Areal capacitance (mF/cm2)
PPy
PMo12@PPy
PW12@PPy
(c)
PPy
PMo12@PPy
PW12@PPy
Specific capacitance (F/g)
Current density (mA/cm2)

Fig. 5

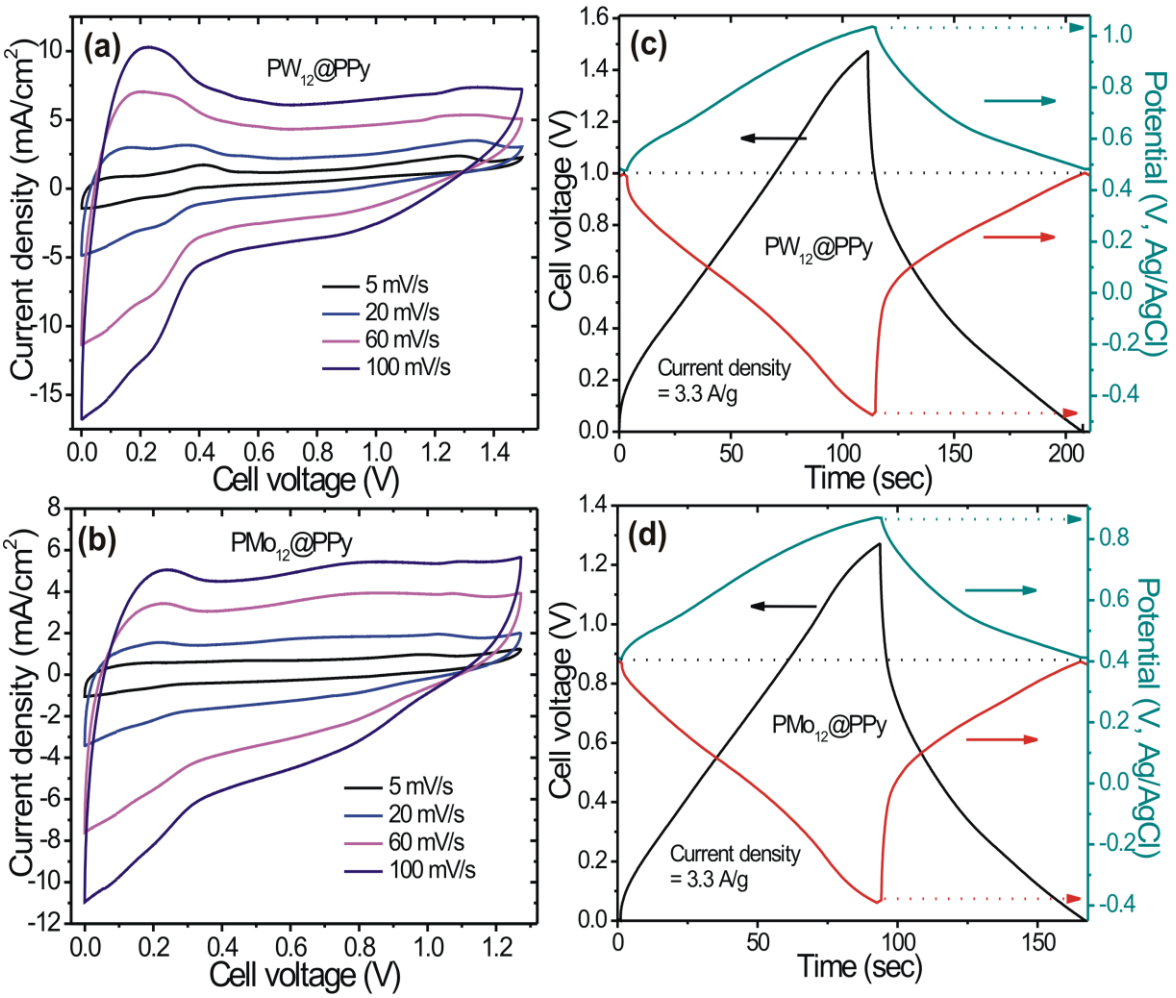
(a)
PW12@PPy
Current density (mA/cm2)
Cell voltage (V)
5 mV/s
20 mV/s
60 mV/s
100 mV/s
(b)
PMo12@PPy
Current density (mA/cm2)
Cell voltage (V)
5 mV/s
20 mV/s
60 mV/s
100 mV/s
(c)
PW12@PPy
Current density
= 3.3 A/g
Cell voltage (V)
Potential (V, Ag/AgCl)
Time (sec)
(d)
PMo12@PPy
Current density
= 3.3 A/g
Cell voltage (V)
Potential (V, Ag/AgCl)
Time (sec)

Fig. 6

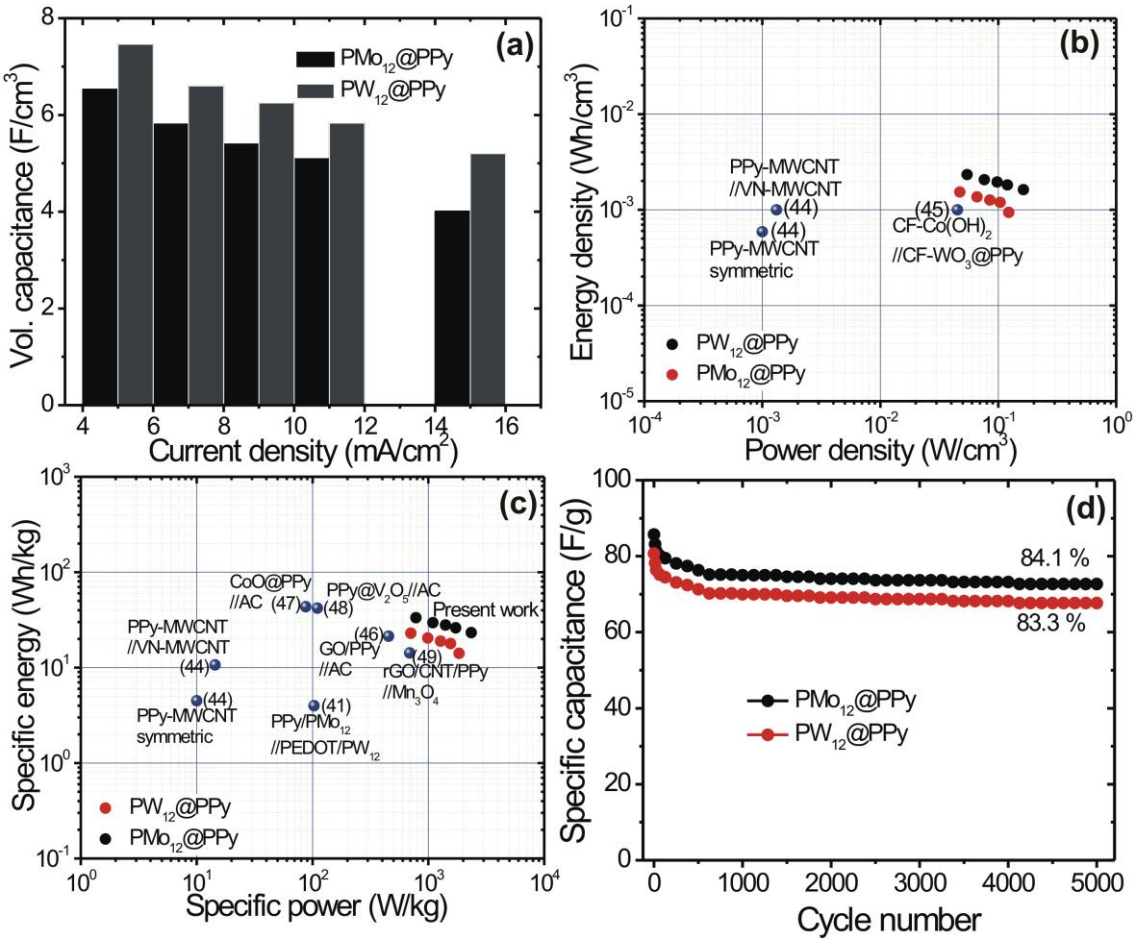
(a)
PMo12@PPy
PW12@PPy
Vol. capacitance (F/cm3)
Current density (mA/cm2)
(b)
PPy-MWCNT //VN-MWCNT (44)
(44) PPy-MWCNT symmetric
(45) CF-Co(OH)2 //CF-WO3@PPy
PW12@PPy
PMo12@PPy
Energy density (Wh/cm3)
Power density (W/cm3)
(c)
CoO@PPy //AC (47)
PPy@V2O5//AC (48)
Present work
PPy-MWCNT //VN-MWCNT (44)
(46) GO/PPy //AC
(49) rGO/CNT/PPy //Mn3O4
(44) PPy-MWCNT symmetric
(41) PPy/PMo12 //PEDOT/PW12
PW12@PPy
PMo12@PPy
Specific energy (Wh/kg)
Specific power (W/kg)
(d)
84.1 %
83.3 %
PMo12@PPy
PW12@PPy
Specific capacitance (F/g)
Cycle number

Fig. 7